Nanotechnology **19** (2008) 235101 (8pp) doi:10.1088/0957-4484/19/23/235101

High throughput cell nanomechanics with mechanical imaging interferometry

Jason Reed[1,4,6], Matthew Frank[2], Joshua J Troke[2], Joanna Schmit[3], Sen Han[3], Michael A Teitell[2,4,5,6] and James K Gimzewski[1,4,6]

[1] Department of Chemistry and Biochemistry, UCLA, 607 Charles Young Drive East, Los Angeles, CA 90095, USA
[2] Department of Pathology and Laboratory Medicine, David Geffen School of Medicine at UCLA, 10833 Le Conte Avenue, Los Angeles, CA 90095-1732, USA
[3] Veeco Instruments, Inc., 2650 E. Elvira Road, Tucson, AZ 85711, USA
[4] California NanoSystems Institute (CNSI), 570 Westwood Plaza, Los Angeles, CA 90095, USA
[5] Jonsson Comprehensive Cancer Center, Institute for Stem Cell Biology and Medicine (ISCBM), and Molecular Biology Institute, David Geffen School of Medicine at UCLA, 10833 Le Conte Avenue, Los Angeles, CA 90095-1732, USA

E-mail: jreed@chem.ucla.edu, mteitell@ucla.edu and gim@chem.ucla.edu

Received 3 December 2007, in final form 7 February 2008
Published 6 May 2008
Online at stacks.iop.org/Nano/19/235101

Abstract
The dynamic nanomechanical properties of a large number of cells (up to hundreds), measured in parallel with high throughput, are reported. Using NIH 3T3 and HEK 293T fibroblasts and actin depolymerizing drugs, we use a novel nanotechnology to quantify the local viscoelastic properties with applied forces of 20 pN–20 nN, a spatial resolution of <20 nm, and a mechanical dynamic range of several Pa up to ~200 kPa. Our approach utilizes imaging interferometry in combination with reflective, magnetic probes attached to cells. These results indicate that mechanical imaging interferometry is a sensitive and scalable technology for measuring the nanomechanical properties of large arrays of live cells in fluid.

(Some figures in this article are in colour only in the electronic version)

1. Introduction

The physical structure of a cell is complex and dynamic, with cytoskeletal elements oriented in many directions, and thus its mechanical properties are highly anisotropic [1, 2], and vary widely among individual cells within a population [3–5]. The degree and significance of cellular mechanical anisotropy and its population variances is poorly characterized, however, due to methodological limitations of existing nanomechanical probing techniques. Existing single-point measurement approaches, such as AFM [6], and high-magnification particle tracking microrheology [7], are simply too slow to adequately measure the number of individual cells required for population comparisons. On the other hand, wide-field magnetic/optical bead tracking methods [4, 8], which rely on beads fixed to the cell surface, can only track the probe with sufficient accuracy (tens of nanometers [8, 9]) in two dimensions (the x–y plane perpendicular to the objective). Therefore, there is a strong need to extend probe-based mechanical measurements into all three dimensions, while retaining measurement accuracy and high throughput.

In this paper, we demonstrate a new nanomechanical probing method, called mechanical imaging interferometry (MII), based on combining vertical scanning interferometry with reflective, magnetic probes attached to cells that permit axially oriented mechanical measurements of live cells with picoNewton force resolution over wide fields of view. We show that mechanical imaging interferometry (MII) has axial position repeatability of <20 nm over a very wide vertical range (millimeters), and can measure materials with elastic moduli over the range of 50 Pa to 100+ kPa. Because the interferometric technique we use is relatively insensitive to magnification, we retain excellent positional resolution at fields of view of up to or exceeding 740 μm × 570 μm, permitting simultaneous measurement of hundreds of probes.

[6] Authors to whom any correspondence should be addressed.

This allows estimated throughput to equal or significantly exceed existing wide-field optical tracking techniques. Unlike these aforementioned methods, MII directly measures the position of the bead on the cell membrane versus the substrate, and thus can determine cell thickness very accurately; this is critical for accurate mechanical modeling of cells in some cases [10]. Using soft polyacrylamide gels of known stiffness, we demonstrate an absolute measurement accuracy equal to that of AFM indentation in a similar experimental configuration (6% standard error on a gel with Young's modulus of 4 kPa, $n = 23$). Using MII we determine the quasi-static mechanical properties of populations of NIH 3T3 and HEK 293T fibroblasts, by probing large arrays of individual cells in parallel. The absolute values of the mechanical constants determined by MII are in excellent agreement with results from other probing methods such as AFM and magnetic twisting cytometry.

Our results show that MII is an effective, high throughput technique for measuring cellular mechanical properties through indentation normal to the cell surface. This represents a significant throughput advance over AFM, and other optical approaches, such as confocal microscopy or microfluidic optical stretchers [11], which cannot accurately measure mechanical properties of large arrays (hundreds) of cells simultaneously, with single-cell specificity [9, 12]. The mechanical dynamic range of MII equals or exceeds comparable optical techniques, and the effective field of view is larger (3× presently) [4]; the limiting field of view for MII has not been established, but technical considerations discussed in this paper suggest it could be much larger (>10×). Finally, these results suggest that MII could be used in combination with traditional optical particle tracking to conduct rapid, fully 3D mechanical probing of large arrays of live cells.

2. Materials and methods

2.1. Interferometer

The measurement of the microreflectors was performed on the Veeco interference microscope NT 1100 with a green diode used for illumination and 20× 0.28 NA Michelson through transmissive media (TTM) objective [13]. The NT 1100 in principle is an optical microscope with a Michelson interference objective that allows for the observation of not only lateral features with typical optical resolution (1.16 μm for the 20× objective) but also height dimensions below the scale of 1 nm [14]. The Michelson interferometer is composed of a beam splitter, reference mirror and compensating fluid cell. The compensation cell is 0.7 mm thick bounded on both sides by 0.5 mm optical windows, thus matching the optical path length of a reflected beam from the sample observation chamber. The CCD detector array is 640 × 480 pixels, which with a 20× objective produces a 315 μm × 240 μm field of view and a spatial sampling of 500 nm. Measured positions of the reflectors with respect to the bottom of the sample chamber were corrected for the effect of dispersion in liquid, using a group velocity at 535 nm wavelength and 30 nm band pass of $Ng = 1.33$ [15].

2.2. Cell perfusion chamber

The chamber was constructed from non-magnetic stainless steel. Resistive heating elements with internal thermistors, driven by a feedback controlled power supply, were used to regulate the chamber temperature to within 0.5 °C. The fluid sample was contained within a 13 mm diameter, 0.7 mm thick sub chamber, having a 1 mm thick optical window on top and a 0.2 mm thick silicon floor. Fluid within the chamber could be exchanged through peripheral infusion ports, using a micro peristaltic pump capable of flow rates as low as 5 μl min^{-1}.

2.3. Microreflectors

Elemental nickel microspheres (2–10 μm dia.) were obtained from Duke Scientific as a dry powder. For each experiment, approximately 0.1 mg of powder was mixed with 1 ml of cell culture media or buffer as described below. Smaller diameter particles were removed by sedimentation, resulting in a dilute suspension with size distribution ∼5–10 μm. One hundred microliters of 0.2% poly-L-lysine aqueous solution (Sigma) was added to the suspension to inhibit aggregation and improve adhesion to the cell bodies. The microreflector suspension was shaken vigorously before application to reduce aggregates. Approximately 200 μl of the suspension was pipetted onto the sample (gel or cells) and the microreflectors allowed to settle for a minute.

2.4. Magnetic force control

Magnetic force was applied to the microreflectors using a cylindrical rare-earth magnet 7 mm in diameter by 21 mm long, oriented axially along the vertical direction below the test chamber. The magnet was positioned with a feedback controlled motorized micrometer, capable of <10 μm accuracy. The magnitude of magnetic flux perpendicular to the vertical axis, as a function of axial distance, was measured with a miniature Hall probe. In the 'off' position, the magnet was lowered to >4 cm below the sample, resulting in negligible field at the sample point. The magnet was positioned coaxially with the optical path to ensure a uniform magnetic flux across the viewing area (∼300 μm × 300 μm with the 20× objective). The force applied to the nickel microreflectors as a function of magnet position was determined using microcantilever arrays tipped with elemental nickel and uniformly magnetic microspheres (Compel 8 μm carboxylated microspheres, Bangs Labs). Each microcantilever was 500 μm long by 100 μm wide and 0.9 μm thick, with a nominal spring constant of 0.01 N m^{-1}. These commercially available arrays were produced by the IBM Zurich Research Laboratories using a proprietary dry etch, silicon-on-insulator (SOI) process. Using the optical profiler, the deflection of the reference cantilever could be determined to better than 1 nm. The volume magnetic moment for pure nickel (55 emu g^{-1}) was assumed for both the microreflectors and the nickel film deposited on the cantilever tips. Pure nickel is completely magnetically polarized at field strengths of 200 G and higher, while the lowest field strength used in measurements was ∼500 G. Preceding measurements, the magnet was raised to within 1.5 mm of the sample,

corresponding to a ∼2 kG flux at the sample point, to ensure that the microreflectors' magnetic moments were oriented axially.

2.5. Polyacrylamide gel tests

5% acylamide/0.15% bis-acrylamide and 5% acrylamide/0.05% bis-acrylamide gels were cast between a microscope slide and cover slip, using 40 μm tape as a spacer, using standard conditions [16]. A 5 mm × 5 mm section of each gel was removed with a scalpel and placed inside the fluid test chamber for measurement. Samples in the test chamber were allowed to equilibrate overnight in 1× Tris-Borate-EDTA (TBE) buffer, pH 7.5, the same buffer used to prepare the gels. All measurements were conducted under buffer.

2.6. Cell viscoelastic measurements

The population measurements of the NIH 3T3 fibroblasts and the HEK 293T fibroblasts were conducted over several consecutive days. Both cell types were cultured simultaneously on a series of poly-L-lysine coated 0.20 mm × 10 mm round glass cover slips, in 1× Dulbecco's Modification of Eagle's medium (DMEM) with 10% fetal bovine serum in a laboratory incubator under standard cell culture conditions. Preceding measurement, a single round cover slip containing cells would be removed from the culture dish and quickly placed in the microscope test chamber. Microreflectors would be added to media from the original culture dish, prepared as described above, which would then be pipetted slowly onto the cells and the sample chamber sealed. Cells were allowed to equilibrate in the test chamber for 30 min before measurement. The average diameter of the measured microreflectors was 7.6 μm, and the average applied force was 190 pN. The average cell height was 6.1 μm and the average maximum indentation depth per cell was 500 nm. The following factors showed no significant difference between the two populations based on ANOVA analysis: cell height, applied force, reflector radius and maximum indentation depth/radius.

The three mechanical constants were determined for each measurement by fitting the time-dependent force–displacement curves of the microreflectors to the following equation for a standard linear viscoelastic solid material [17]:

$$\delta(t) = \frac{3}{4}\sqrt[3]{3F^2/4RE_1^2}\left\{\left(-\frac{E_1}{E_2}\mathrm{e}^{-(E_2 t/3\eta)}\right)+\left(\frac{E_1+E_2}{E_2}\right)\right\}^{2/3}$$

where $\delta(t)$ is the displacement as a function of time, t; F is force applied to the microsphere with radius R; η is the viscosity of the material and E_1 and E_2 are the elastic moduli of the material. We used a commonly assumed value for the Poisson's ratio of a mammalian cell, $\nu = 0.5$, which is the relation between shear and compression stretching for an incompressible material [18]. Experiments suggest that the Poisson's ratio for fibroblasts is typically in the range of 0.4–0.5 [6]. Curves were fitted using the Levenberg–Marquardt non-linear least squares procedure (Origin Labs). The z-statistic was used to compare the log-transformed sample means and determine p values. The Bartlett test was used to confirm homogeneity of the compared sample variances. To remain within the semi-infinite layer assumptions of this model, we present fits only for observations where the minimum cell thickness at the location of the microreflector was 3 μm or greater. For the elastic constants E_1 and E_2, most of the fits had a relative standard error of fit <25%. This level of uncertainty is small in comparison to the expected variation in elasticity within a 'homogeneous' cell population, which can be three orders of magnitude (see section 3), and is sufficiently accurate to allow comparisons between populations. There was larger uncertainty in the viscosity factor, η, with only 30% of the fits having a relative standard error <25%. The error in η is mainly due to the temporal sampling rate of 0.1 Hz, which did not adequately resolve the rapid indentation of the microreflectors on the softest cells.

2.7. Cytochalasin B measurements

Cells were prepared for measurement as described above. A continuous infusion of fresh media into the sample chamber, warmed to 37 °C and pre-saturated with 5% CO_2, was maintained at all times. The rate of infusion was 5 μl min^{-1}, equivalent to exchanging the entire volume of the test chamber in 20 min. Cells were equilibrated under flow for 45 min before measurement. Flow was halted during each measurement cycle, which lasted approximately 200 s. A media-only measurement was conducted first, followed by introduction of cytochalasin B into the infusing media. Initially, the cytochalasin B was dissolved in dimethyl sulfoxide (DMSO) and diluted in DMEM to produce a stock concentration 1000× the working concentration (1 μM or 10 μM).

2.8. Repeatability and throughput

In our experiments, the range of forces generated on a typical microreflector (8 μm dia.) was 20 pN up to 20 nN, depending on the applied magnetic field. The repeatability of our axial measurements of microreflector position versus the substrate, a distance of severalμm, was roughly 20 nm. Therefore, using the Hertz model for a spherical indenter [18], the maximum repeatability of our elasticity measurements was roughly 5%, assuming that the bead diameter and magnetic force were determined to high precision (<0.5%).

In both MII and standard wide-field bead tracking experiments, for a given bead diameter and measurement time, throughput is limited by the number of probes in the field of view. We were able to obtain measurement precision of <20 nm using a 20× 0.28 NA objective and a 0.5× demagnifier, with a CCD detector array having 640 × 480 pixels, which produced a 600 μm × 440 μm field of view and a spatial sampling of 952 nm. In comparison, wide-field optical magnetic twisting cytometry (OMTC) [4] uses a 10× 0.2 NA objective and a camera with 780 × 600 pixels, which produces a 450 μm × 350 μm field of view and a spatial sampling of 570 nm per pixel. Therefore, if we used a CCD with 780 × 600 pixels and the same 952 nm spatial sampling, we would obtain a field of view of 742 μm × 571 μm, which equates to roughly 3× the measurement area versus OMTC.

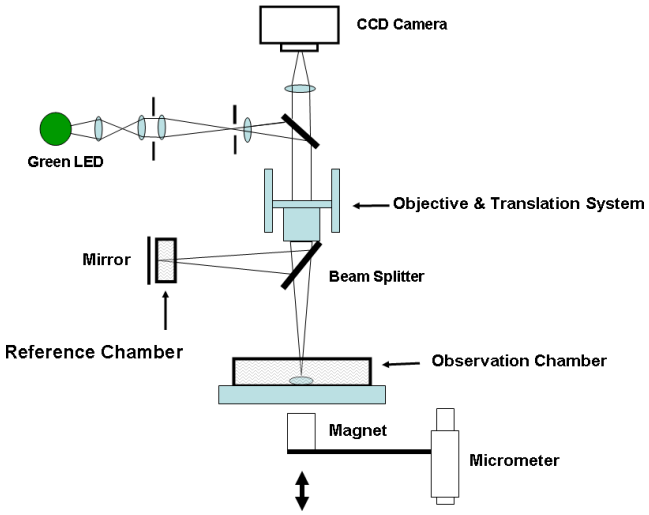

Figure 1. The interferometric microscope. The microscope can accommodate a 5× and 20× long-working distance microscope objective. Below the objective is the Michelson interferometer with an adjustable mirror in the reference arm. A fluid compensation cell was positioned in the interferometer's reference arm to permit measurements inside the media-filled observation chamber. Dimensions of the compensation cell were adjusted to exactly match the optical path length between the test and reference arms. A cylindrical rare-earth magnet mounted on a micrometer was positioned below the cell chamber. The magnitude of the magnetic force applied to the nickel microreflectors inside the observation chamber was adjusted by varying the distance between the magnet pole face and the sample.

3. Results and discussion

Mechanical imaging interferometry (MII) makes use of spherical microreflectors fixed to the cell membrane that act as nanoscopic displacement probes. We utilized a modified interferometric microscope, combined with a specially constructed perfusion chamber for these measurements. Figure 1 shows a schematic of the apparatus. Measuring live cells in culture required the placement of a liquid-filled compensation chamber in the reference arm of the interferometer. Dimensions of the compensation chamber were adjusted to match exactly the optical path length between the test and reference arms. Cells were evaluated in a sealed environmental chamber maintained at 5% CO_2, 37 °C, with infusion ports for exchanging media and the introduction of drugs and other chemicals. The microreflectors were pure nickel, ranging from 6 to 10 μm in diameter.

During each measurement, the focus point is scanned vertically from the surface to a height of 40 μm above the surface, such that each point in the volume passes through focus. The interferometer is aligned so that the interference intensity distribution along the vertical scanning direction has its peak (best fringe contrast) at approximately the best focus position. The vertical-axis position of each microreflector is determined as the location of the coherence peak within the scan. By measuring microreflectors of known height fixed to a solid substrate in liquid, we determined that the z-axis measurement repeatability was <20 nm. Magnetic forces applied to the nickel microspheres were calibrated with a ferromagnetic-tipped microcantilever array, having a known spring constant and magnetic moment. The range of forces achievable on an 8 μm diameter nickel microreflector was approximately 20 pN up to 20 nN. A critical consideration for cell nanomechanical measurements is the dynamic range of the measurement technique. Mammalian cells exhibit a wide range of Young's moduli, from as soft as 10 Pa to as stiff as 100 kPa [19]. We estimate that MII can effectively measure samples with elastic moduli that vary from several Pa up to ∼200 kPa, as currently configured.

To validate our approach, we first tested the microreflectors on 40 μm thick, soft polyacrylamide (PA) gels under liquid, which simulated the cell body (figure 2). We recorded the vertical displacement of the microspheres in response to a series of increasing forces. The resulting force–displacement curves fit the Hertz contact model [18] for a spherical indenter well. The measured values for Young's modulus were linearly proportional to the cross linker concentration, as expected, and the range of absolute values and measurement precision (1530 s.e. ±128 Pa, $n = 22$ and 4020 s.e. ±270 Pa, $n = 23$) agree well with similar measurements by others using AFM and bulk techniques [6, 20, 21].

Next, we measured the mechanical properties of live mouse NIH3T3 and human HEK293T fibroblasts. In the perfusion chamber, the microreflectors on top of individual cells or cell layers appeared as distinct objects in the interferometer image (figure 3). Similar to the PA gel tests, we applied a series of step forces and recorded vertical reflector displacements. The indentation and recoil was proportional to the applied force, as expected, but the cell bodies showed a distinct viscoelastic response, versus the purely elastic behavior of the PA gels. This is most clearly seen as 'creep behavior' of the microreflectors in response to a step change in force (figure 4).

Live cells are known to exhibit complex frequency-dependent viscoelastic properties [22–24]. For the purpose of this study we were primarily interested in determining the equilibrium elastic modulus of the cells. To this end, we used a 3-factor linear viscoelastic solid model to parameterize the cell's response [17]. This type of model has been used to characterize the viscoelastic properties of cells and soft polymers [18]. It consists of two springs and a dashpot, specified by two elastic constants (E_1, E_2) and one viscous constant (η) (figure 4). The stress-bearing capacity of the cytoskeleton is represented by a short term-response, E_1, and a slower response, E_2. The response of the spring element E_2 is delayed by viscous drag. Our ability to resolve the viscous constant is limited by the 0.1 Hz temporal sampling rate, but this does not influence our ability to measure the equilibrium elasticity, which is given by E_1 and E_2. A full temporal characterization of the cellular viscoelastic response is beyond the scope of this study, however, as we discuss below, MII is fully compatible with the cyclic probing methods commonly used to determine frequency-dependent mechanical moduli. For both cell types, the population distributions of the viscoelastic constants were log-normally distributed, with geometric standard deviations of ∼1.5 logs. This result is in agreement with recent reports [4, 19, 25]. The means and

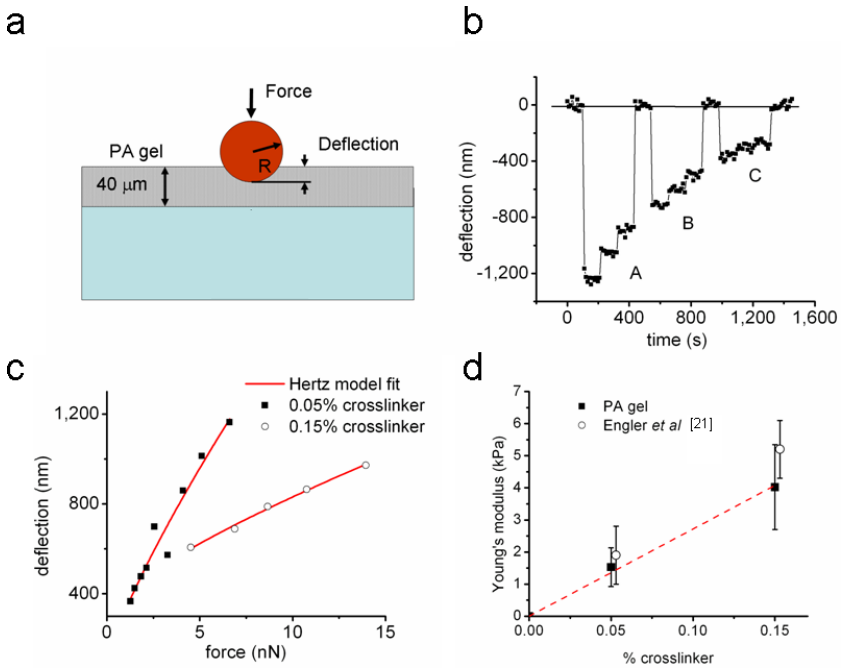

Figure 2. (a) Geometry of the force-indentation tests using a 40 μm thick polyacrylamide (PA) gel to simulate the cell body. (b) A force–distance curve showing the deflection of a 7 μm dia. nickel microreflector into a 0.05% crosslinker PA gel under a series of decreasing forces: A = 6.6, 5.3 and 4.2 nN; B = 4.2, 3.3, 2.8 nN; C = 2.4, 1.9 and 1.6 nN. (c) Force–distance measurements were fitted to the Hertz contact model for a spherical indenter, from which the gel's elastic modulus was calculated. Data points from individual measurements on a 0.05% and a 0.15% crosslinker gel show the correspondence between the force–deflection behavior of the microreflectors and that predicted by the Hertz model. (d) The measured values for Young's modulus were linearly proportional to the crosslinker concentration, as expected, and the ranges of absolute values (1530 $\pm$ 600 Pa and 4020 $\pm$ 1300 Pa) agree well with similar measurements by others using AFM and bulk techniques [6, 20, 21].

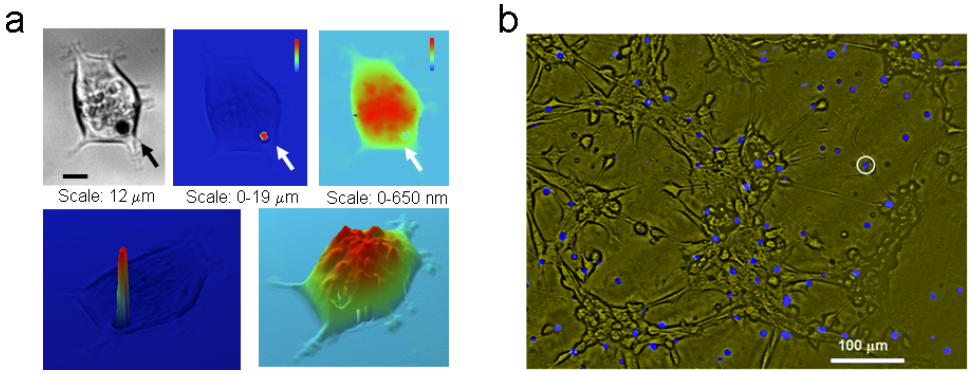

Figure 3. (a) Top: intensity image of an NIH 3T3 fibroblast (left) with a microreflector positioned on the cell membrane (arrow). The corresponding interferometric height profile (middle) includes only the microreflector since the cell body is not reflective. The phase image (right) shows the cell body, where apparent height corresponds to increased optical path length due to the higher index of refraction of the cytoplasm versus the surrounding media. The use of interferometric phase measurements with this apparatus is detailed in [13]. The microreflector is opaque and does not appear in the phase image. Bottom: the interferometric height and phase profiles are rendered in 3D for clarity. (b) An intensity image of NIH 3T3 fibroblasts in the observation chamber taken at 10$\times$ magnification; the field of view is 600 μm $\times$ 460 μm. The interferometric image is overlaid in blue, showing the detection of 103 microreflectors (an example is indicated with the white circle).

standard errors of the log-transformed pooled measurements for both cell types are shown in figure 5. The mechanical constants for the HEK293T cells are consistently lower than for the NIH3T3 cells, although the difference was statistically significant at the >95% level only for the delayed elastic constant E_2.

We evaluated the behavior of NIH3T3 cells ($n = 30$) exposed to a low dose (1 μM) of cytochalasin B, which inhibits actin polymerization. At low doses (0.1–1 μM), cytochalasin B does not produce large changes in the morphology of fibroblasts, although it does inhibit cell migration [26, 27]. In agreement with other reports [26], we found that cells treated with low doses of the drug were slightly more elastic (figure 6). For the population, the mean of the log-transformed distribution of E_1 was 3.19 before treatment and 2.92 after ($p = 0.10$). Similarly, the means of E_2 were 2.30 before

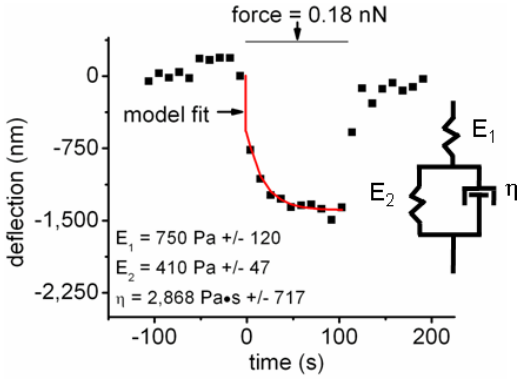

Figure 4. (a) A force–distance curve showing the deflection of a 10 μm microreflector into a single HEK293T cell. The viscoelastic nature of the cell body is apparent from the delay between the onset of force change and the time required to reach an equilibrium deflection (creep). This creep behavior can be represented by a simple three-factor viscoelastic solid model, consisting of two springs and a dashpot (inset). This model contains an instantaneous elastic constant, E_1, and a time-delayed elastic constant, E_2. The time delay is governed by the magnitude of E_2 and the viscosity, μ. The three viscoelastic constants can be calculated by fitting the observed force–deflection curve to a version of the three-factor model applicable to spherical indenter geometry [17].

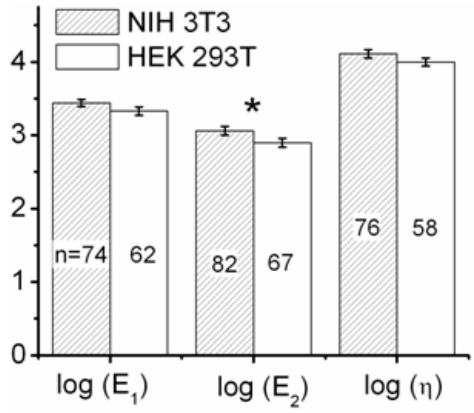

Figure 5. The population distribution of the three viscoelastic constants determined for populations of NIH 3T3 and HEK 293T fibroblasts. The error bars indicate standard error of the mean, and * indicates statistical significance at the >95% level. The means of the log-transformed distribution of E_1 were 3.45 for NIH3T3 and 3.33 for HEK293T fibroblasts ($p = 0.10$). The means of the log-transformed distributions of E_2 were 3.06 and 2.90 ($p = 0.03$), and the means of the log-transformed viscous constants η were 4.11 and 4.00 ($p = 0.17$), respectively.

and 2.02 after ($p = 0.04$), and the means of the viscous constants η were 3.39 before and 3.36 after ($p = 0.47$). While the population difference was statistically significant only for E_2, on a matched, individual cell basis, the elasticity was consistently lower after treatment (E_1 10/13 lower, E_2 7/10 lower), while viscosity was not (η 6/11 lower). Qualitatively, 1 μM cytochalasin produced only a slight change in cell morphology up to 45 min, as expected, while the indentation profiles show a clear change in some cells and not in others (cells 2 and 3 in figure 6(b)).

Our measurements of live fibroblast cells provide a direct comparison of MII to AFM and other nano-indentation methods. The magnitude of the elastic constants and the response to cytochalasin B determined by MII were in excellent agreement with reported results for fibroblasts, determined by AFM, bead tracking microrheology and microplate traction [18]. The temporal sampling rate in our experiments was 0.1 Hz, effectively limiting our mechanical measurements to quasi-static. Therefore, while the average viscous constant we determined for both fibroblast cell types is similar to that reported by other methods [18, 28], we cannot effectively determine η or cells with a very low viscosity ($<\sim$1 kPa s). This resulted in the relatively larger error in fitting the viscous constant versus the elastic constants in our three-factor mechanical model.

On the other hand, MII is very well suited to investigate longer timescale mechanical responses, including 'active' behavior such as cytoskeletal remodeling and cell motility. This is because unlike most competing technologies, it does not require the filtering out of low frequency motions to achieve accuracy, and the absolute height of the probe over the substrate is measured with high precision (<0.2%) every measurement cycle. In fact, a subset of the creep curves we recorded showed time-varying behavior consistent with an active mechanical response, such as the cell lifting the microreflector several hundred nanometers while under load. The duration of the force cycle, 100 s, was within the timescale of active mechanical responses by the cell, such as lamellepodial extension/retraction (tens of seconds or more), and cytoskeletal tensioning by molecular motors (minutes) [29, 30].

To date, optical magnetic twisting cytometry (OMTC) [1, 4, 8, 31] is the only other technique capable of measuring the mechanical properties of individual live cells with a throughput and sensitivity comparable to MII. The primary difference between the two methods is that with MII the mechanical properties of the cell are measured by indentation perpendicular to the cell surface, whereas OMTC measures mechanical shear in the x–y plane of the cell membrane. Aside from the orientation-specific mechanical information obtained, measurement by z-axis indentation versus surface twisting (shearing) has several advantages. It does not require that the probe be tethered to cell surface receptors as in the case of twisting measurements [8], and because the magnetizing force and the indenting force are aligned in MII, there is no limit to the maximum magnetic field which can be applied. In OMTC, the actuating (twisting) field is perpendicular to the probe's magnetic moment, and thus is limited to less than $\sim$100 G in order to avoid demagnetizing the probe. In both methods, the measurement of absolute mechanical constants requires assumptions about the probe–cell contact area that are difficult to validate *in situ*; this is a concern common to magnetic/optical bead twisting and pulling methods, as well as AFM in some cases.

We estimate that both methods have a similar dynamic range of measurable elastic moduli, from tens of Pascals to 100+ kPa. The effective throughput, which is limited by the field of view, is several-fold larger for MII versus OMTC.

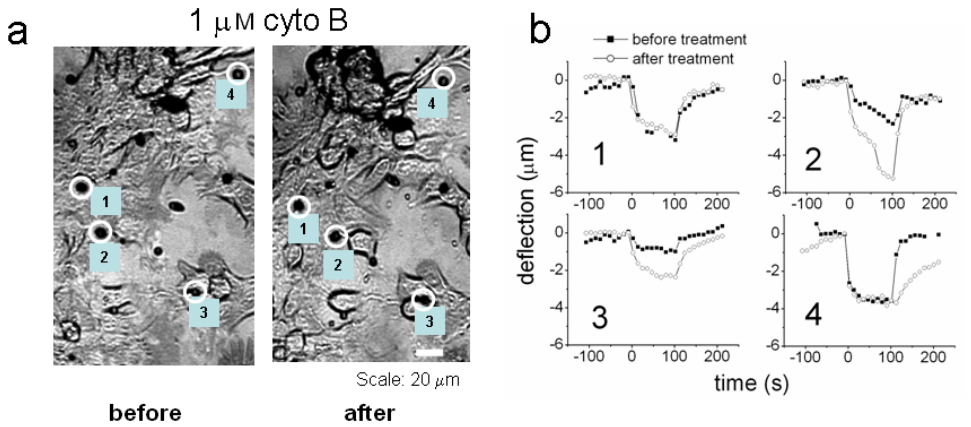

Figure 6. (a) Intensity images of NIH3T3 cells with microreflectors in place, before and after treatment with 1 μM cytochalasin B. (b) The force–displacement curves of four individual microreflectors before and after treatment shows the change in viscoelastic behavior in response to normal force applied for 100 s (t = 0–100 on the graphs). Probes 2 and 3 show a clear decrease in stiffness, while probe 4 shows a change in elastic rebound behavior, and probe 1 appears to be unchanged. The force generated on the cell by each nickel microreflector is a function of the probe's total mass: (1) radius = 3.85 μm, force = 180 pN; (2) radius = 3.90 μm, force = 190 pN; (3) radius = 3.40 μm, force = 130 pN; (4) radius = 4.75 μm, force = 340 pN.

OMTC claims positioning accuracy of 5–10 nm versus 10–20 nm for MII [4], using phase-locked detection, which is also implementable in MII. Unlike OMTC, AFM, and some other optical techniques, MII determines absolute cell height every measurement, to ∼0.3% accuracy, and has a vertical range of millimeters. This allows MII to capture dynamic changes in cell shape and multi-cell structures, without compromising sensitivity. Also, knowing the thickness of the cell below the probe is critical to accurate mechanical modeling of cells in some cases [10].

OMTC utilizing phase-locked detection has a wide temporal dynamic range, from 0.01 to 100+ Hz. Our study utilized a temporal sampling rate of 0.1 Hz. However, this is not a fundamental limitation of MII. We have used phase-locked detection to measure nanometer motion of MEMS structures up to 1 MHz with the MII optical system [32], and we expect that this could easily be translated to live cell measurements.

Finally, MII may prove to be more scalable than OMTC, which has been optimized over several years to achieve spatial sensitivity of 5–10 nm, or 0.008 fractional pixels, which studies suggest is at or near the practical limit of non-interferometric particle tracking [9, 12]. On the other hand, the accuracy of measurement in the z-axis using vertical scanning interferometry is theoretically insensitive to magnification for surfaces with low curvature [14, 33]. At its limit, interferometric microscopy can operate with magnifications as low as 1×, or approximately 5 mm × 5 mm field of view. With this level of resolution using microreflectors, spherically shaped or otherwise, it is possible to perform cell mechanical measurements simultaneously over an area in excess of 600× conventional methods. This would enable longitudinal time studies of mechanical properties, where not only single-cell, but also simultaneous cell–cell interaction and the effect of long-scale (hundreds of microns) physical or chemical gradients can be observed.

4. Conclusions

The primary conclusions of this study are as follows: MII is capable of axially tracking magnetic microreflectors, with <20 nm spatial precision, in the optically complex environment of live cell culture. Using MII we have measured the elastic moduli of live cells through nano-indentation. MII attained excellent positional resolution at low effective magnification (spatial sampling ∼500–900 nm per pixel), permitting simultaneous measurement of up to 100 probes. Our results indicate that MII has a wide mechanical dynamic range, from several Pa up to ∼100 kPa, and can achieve a 20 pN–20 nN range of forces on a typical microreflector.

Using soft polyacrylamide gels of known stiffness, we quantitatively demonstrate an absolute measurement accuracy exceeding that of AFM indentation in a similar experimental configuration (6% standard error on a gel with Young's modulus of 4 kPa, n = 23). Using MII we also determined the quasi-static mechanical properties of populations of NIH 3T3 and HEK 293T fibroblasts, where the absolute values of the mechanical constants were in excellent agreement with results from other nanomechanical probing methods.

Our results show that MII achieves high throughput when measuring cellular mechanical properties using indentation normal to the cell surface. This represents a significant throughput advance over AFM, and other optical approaches, such as confocal microscopy or microfluidic optical stretchers, which cannot accurately measure mechanical properties of large arrays (hundreds) of cells simultaneously, with single-cell specificity [9, 12]. The mechanical dynamic range and effective magnification of MII equals or exceeds existing wide-field optical particle tracking techniques [4], which implies that the two could be used in combination to conduct rapid, fully 3D mechanical probing of large arrays of live cells.

Acknowledgments

This study was funded by NIH grant R21GM074509. Additional support was provided by the NIH Roadmap for Medical Research PN2EY018228, NIH grants R01CA90571, R01CA107300, R01GM073981. MAT is a Scholar of the Leukemia and Lymphoma Society.

References

[1] Smith P G, Deng L H, Fredberg J J and Maksym G N 2003 Mechanical strain increases cell stiffness through cytoskeletal filament reorganization *Am. J. Physiol. Lung Cell. Mol. Physiol.* **285** L456–63

[2] Hu S H *et al* 2003 Intracellular stress tomography reveals stress focusing and structural anisotropy in cytoskeleton of living cells *Am. J. Physiol. Cell Physiol.* **285** C1082–90

[3] Fabry B, Maksym G N, Butler J P, Glogauer M, Navajas D and Fredberg J J 2001 Scaling the microrheology of living cells *Phys. Rev. Lett.* **87** 148102

[4] Fabry B *et al* 2001 Signal transduction in smooth muscle—selected contribution: time course and heterogeneity of contractile responses in cultured human airway smooth muscle cells *J. Appl. Physiol.* **91** 986–94

[5] Cross S E, Jin Y S, Rao J and Gimzewski J K 2007 Nanomechanical analysis of cells from cancer patients *Nat. Nanotechnol.* **2** 780–3

[6] Mahaffy R E, Park S, Gerde E, Kas J and Shih C K 2004 Quantitative analysis of the viscoelastic properties of thin regions of fibroblasts using atomic force microscopy *Biophys. J.* **86** 1777–93

[7] Weihs D, Mason T G and Teitell M A 2006 Bio-microrheology: a frontier in microrheology *Biophys. J.* **91** 4296–305

[8] Mijailovich S M, Kojic M, Zivkovic M, Fabry B and Fredberg J J 2002 A finite element model of cell deformation during magnetic bead twisting *J. Appl. Physiol.* **93** 1429–36

[9] Cheezum M K, Walker W F and Guilford W H 2001 Quantitative comparison of algorithms for tracking single fluorescent particles *Biophys. J.* **81** 2378–88

[10] Dimitriadis E K, Horkay F, Maresca J, Kachar B and Chadwick R S 2002 Determination of elastic moduli of thin layers of soft material using the atomic force microscope *Biophys. J.* **82** 2798–810

[11] Guck J *et al* 2005 Optical deformability as an inherent cell marker for testing malignant transformation and metastatic competence *Biophys. J.* **88** 3689–98

[12] Carter B C, Shubeita G T and Gross S P 2005 Tracking single particles: a user-friendly quantitative evaluation *Phys. Biol.* **2** 60–72

[13] Reed J, O Doherty K, Schmit J, Han S, Troke J, Teitell M, Klug W and Gimzewski J 2006 Applications of imaging interferometry *Proc. SPIE—Int. Soc. Opt. Eng.* **6293** 629301 0277-786X

[14] Olszak A G, Schmit J and Heaton M G 2001 Interferometric approaches each have advantages *Laser Focus World* **37** 93–5

[15] Millard R C and Seaver G 1990 An index of refraction algorithm for seawater over temperature, pressure, salinity, density, and wavelength *Deep-Sea Res.* A **37** 1909–26

[16] Engler A J, Richert L, Wong J Y, Picart C and Discher D E 2004 Surface probe measurements of the elasticity of sectioned tissue, thin gels and polyelectrolyte multilayer films: correlations between substrate stiffness and cell adhesion *Surf. Sci.* **570** 142–54

[17] Cheng L, Xia X, Scriven L E and Gerberich W W 2005 Spherical-tip indentation of viscoelastic material *Mech. Mater.* **37** 213–26

[18] Lim C T, Zhou E H and Quek S T 2006 Mechanical models for living cells—a review *J. Biomech.* **39** 195–216

[19] Balland M *et al* 2006 Power laws in microrheology experiments on living cells: comparative analysis and modeling *Phys. Rev.* E **74** 021911

[20] Mahaffy R E, Shih C K, MacKintosh F C and Kas J 2000 Scanning probe-based frequency-dependent microrheology of polymer gels and biological cells *Phys. Rev. Lett.* **85** 880–3

[21] Engler A, Bacakova L, Newman C, Hategan A, Griffin M and Discher D 2004 Substrate compliance versus ligand density in cell on gel responses *Biophys. J.* **86** 617–28

[22] Trepat X *et al* 2007 Universal physical responses to stretch in the living cell *Nature* **447** 592-U7

[23] Lenormand G, Millet E, Fabry B, Butler J P and Fredberg J J 2004 Linearity and time-scale invariance of the creep function in living cells *J. R. Soc. Interface* **1** 91–7

[24] Desprat N, Richert A, Simeon J and Asnacios A 2005 Creep function of a single living cell *Biophys. J.* **88** 2224–33

[25] Maksym G N *et al* 1999 Mechanical impedance of activated human airway smooth muscle cells from 0.05 to 0.2 Hz *Am. J. Respir. Crit. Care Med.* **159** A470

[26] Rotsch C and Radmacher M 2000 Drug-induced changes of cytoskeletal structure and mechanics in fibroblasts: an atomic force microscopy study *Biophys. J.* **78** 520–35

[27] Yahara I, Harada F, Sekita S, Yoshihira K and Natori S 1982 Correlation between effects of 24 different cytochalasins on cellular structures and cellular events and those on actin *in vitro J. Cell Biol.* **92** 69–78

[28] Koay E J, Shieh A C and Athanasiou K A 2003 Creep indentation of single cells *Trans. ASME J. Biomech. Eng.* **125** 334–41

[29] Tamada M, Sheetz M P and Sawada Y 2004 Activation of a signaling cascade by cytoskeleton stretch *Dev. Cell* **7** 709–18

[30] Giannone G, Dubin-Thaler B J, Dobereiner H G, Kieffer N, Bresnick A R and Sheetz M P 2004 Periodic lamellipodial contractions correlate with rearward actin waves *Cell* **116** 431–43

[31] Maksym G N *et al* 2000 Mechanical properties of cultured human airway smooth muscle cells from 0.05 to 0.4 Hz *J. Appl. Physiol.* **89** 1619–32

[32] Reed J, Wilkinson P, Schmit J, Klug W and Gimzewski J K 2006 Observation of nanoscale dynamics in cantilever sensor arrays *Nanotechnology* **17** 3873–9

[33] Olszak A and Schmit J 2003 High-stability white-light interferometry with reference signal for real-time correction of scanning errors *Opt. Eng.* **42** 54–9